High-capacity organic cathode boosted by coordination chemistry for energy-dense aqueous zinc-organic batteries

Guanzhong Ma[1,†], Zhengyu Ju[2,†], Yutong Chen[1], Runmo Wang[1], Zihao Yuan[1], Huiping Du[1], Mian Cai[1], Meng Gao[1], Yaqun Wang[1,] and Guihua Yu[2,*]*

[1]College of Energy Storage Technology, Shandong University of Science and Technology, Qingdao 266590, China

[2]Materials Science and Engineering Program and Walker Department of Mechanical Engineering, The University of Texas at Austin, TX, 78712, USA.

*To whom correspondence may be addressed.

[†]These authors contributed equally to this work.

Email: yqwang@sdust.edu.cn (Y.W.), ghyu@austin.utexas.edu (G.Y.)

This PDF file includes:

Supporting Information Text

Proposed reaction of TBQPH@GO/Zn cells in aqueous electrolytes

The common ionic embedding mechanisms when organic cathode materials act as cathodes are classified into various types, such as H^+-dominated,[1] Zn^{2+}-dominated,[2] H^+ and Zn^{2+} co-embedded, and anionic embedding.[3] The ionic embedding behaviour of the TBQPH@ material in the electrolyte was analysed by experimental and computational methods. Firstly, since the imine group carries hydrogen atoms at the beginning of the synthesis of the TBQPH material, the imine group will not show reactive activity during the first-turn discharge, so the first-turn discharge is due to the electrochemical behaviour of the carbonyl group reduction, and when the charging is done, both the imine group and the carbonyl group will show electrochemical activity, and the imine group will be stripped of the hydrogen atoms, which will ultimately result in the fully oxidized TBQPH@GO material. At this point, the material will exhibit 10 electron transfer properties. And with the second turn of the discharge, the imine group and carbonyl group will co-store Zn^{2+}, showing a highly synergistic effect, and by the way of DFT calculations and experiments. To verify its ion embedding mechanism during discharge, Zn^{2+} embedding occurs in the first plateau. In addition, the modified TBQPH@GO exhibits superior electrochemical activity and cycle life. Exhibiting ultra-high capacity contribution of 445 mAh g^{-1} at a current density of 0.2 A g^{-1} and 200 mAh g^{-1} at a current density of 10 A g^{-1}, while maintaining 80% capacity retention after 15,000 cycles.

Materials

2,3-Diaminonaphthalene 1,4-dione (DANQ) (97%) was purchased from Macklin (China), tetrachlorobenzoquinone (TCBQ) (99%) was purchased from adamas-beta (China), pyridine was purchased from Macklin (China), zinc sulphate was purchased from Macklin (China), graphene oxide was purchased from Aladdin Biochemical Technology Co. (China), conductive carbon black was purchased from Pioneer Nanomaterials Technology Co., Ltd (China), polyvinylidene fluoride (PVDF) was purchased from Cogent Materials Technology Co.

Synthesis of TBQPH

Disperse and dissolve 0.97 g of DANQ into 50 ml of pyridine, followed by the addition of 0.63 g of TCBQ. Stir the mixture at room temperature for a duration of 36 hours, then perform centrifugation to obtain a brown-red solid. Subsequently, wash the obtained solid with deionized water multiple times before subjecting it to drying at 80 ℃ for a period of 12 hours, resulting in the formation of the brown-red TBQPH product (0.768 g, yield 48%).

Synthesis of TBQPH@GO

Disperse and dissolve 0.97 g of DANQ in 50 ml of pyridine, followed by the addition of 0.63 g of TCBQ, stirring for 6 hours at room temperature. Subsequently, introduce 0.1 g of graphene

oxide and disperse it ultrasonically before continuing to stir for and additional duration of 30 hours. The resulting mixture was subjected to centrifugation, yielding a brownish-red solid that underwent multiple washes with deionized water and subsequent drying in an oven at 80 ℃ for a period of 12 hours. This procedure led to the formation of TBQPH@GO (0.6 g, yield 51%).

Battery assembly

TBQPH@GO //Zn battery: prepared TBQPH@GO The material is uniformly mixed with conductive carbon and PVDF in a ratio of 8:1:1 (weight ratio), and uniformly coated onto a titanium foil current collector with a controlled loading of about 1 mg cm^{-2} and 20 mg cm^{-2}. The mixture is placed in a vacuum oven for 8 hours, and the dried material can be combined with zinc foil to form a battery, with 1 M ZnSO4 as the electrolyte.

Characterizations

FTIR test was performed by Bruker FTIR920, Raman test was performed by Thermo Scientific DXR2, XPS test was performed by Thermo Scientific ESCALAB-250, TEM test was performed by Thermo Scientific FEI Talos F200S, UV spectrophotometer was performed by Agilent Cary 60, SEM test was performed by Thermo Scientific Apero S HiVac, NMR test was performed by Thermo Scientific K-Alpha.

UV-vis analysis

The material was utilized for the fabrication of a battery featuring a zinc negative electrode, while the electrolyte employed was 1 M $ZnSO_4$. This specific concentration of 1 M $ZnSO_4$ electrolyte served as a reference point to monitor alterations in the electrolyte's characteristics subsequent to subjecting the battery to 1000 cycles within the wavelength range of 200 - 800 nm.

Eletrochemical measurements

The TBQPH@GO electrode was prepared by mixing TBQPH@GO, conductive additives and PVDF binder in NMP at a weight ratio of 8:1:1. Subsequently, the resulting slurry was drop-coated onto a carbon cloth with an area of 1 cm^2 and vacuum dried for 12 h. The loading mass of the active substance was approximately 1.0 mg cm^{-2}. A cell assembly was constructed us metal zinc foil as the counter electrode, while the electrolyte consisted of 1 M $ZnSO_4$ solution. CV and EIS tests were conducted using a VMP3 electrochemical workstation from Bruker, Germany; whereas GCD tests were conducted employing a battery testing system (CT-4008-5V1A-S1, Shenzhen Neware, China).

Kinetics studies

The charging and discharging kinetics of TBQPH in aqueous zinc batteries were investigated through CV tests conducted at various scan rates. The CV curves exhibited three pairs of redox peaks, with the peak current (i) and scan rate (v) following the relationship $i = av^b$, where coefficients a and b are determined. In the case where a b value of 0.5, it indicates a diffusion-

controlled process, while a value of 1 indicates a non-diffusion-controlled process. By extracting the peak currents at different scan rates and plotting them against the corresponding scan rate values, we obtained the slope of the this linear fit to determine coefficient b.

DFT calculations

The molecular orbital energy levels of DANQ/TBQPH, including the highest occupied molecular orbital (HOMO) lowest unoccupied molecular orbital (LUMO) energy level, the f+ value of the Fukui function (FUKUI), have been investigated at the B3LYP-D3/TZVP level of theory by using the Dmol3 programme. Electrostatic potential (ESP). Negative potentials (red) indicate electrophilicity, while positive potentials (blue) indicate nucleophilicity，and visualised using VMD software.

The charge storage mechanism of TBQPH was investigated using Materials Stduio with SDD basis set for Zn atoms and 6-31 G(d, p) basis set for C, H, O and N atoms, with the maximum force and energy convergence criteria in the structural optimisation of 0.02 eV A^{-1} and 10^{-6} eV, respectively, and the maximum atomic travel distance of 0.005 A. Using the same methodology, the frequency calculations to determine the true local minima and to obtain thermodynamic data at P=1atm and T=298.15K. The results from this analysis are utilized in determining enthalpy (H), entropy (S), free energy (G) and constant pressure heat capacity (Cp) as functions of temperature.

The Gibbs free energy is calculated as follows:

$$\Delta G^{298.15k} = E_{products}^{298.15K} - E_{reactants}^{298.15K} - x\ (Zn^{2+298.15K}/H^{+298.15K})$$

where X is the number of bound Zn^{2+} or H^{+}.

Figure S1.

Figure S1 NMR images of TBQPH material: H atomic spectrum.

Figure S2.

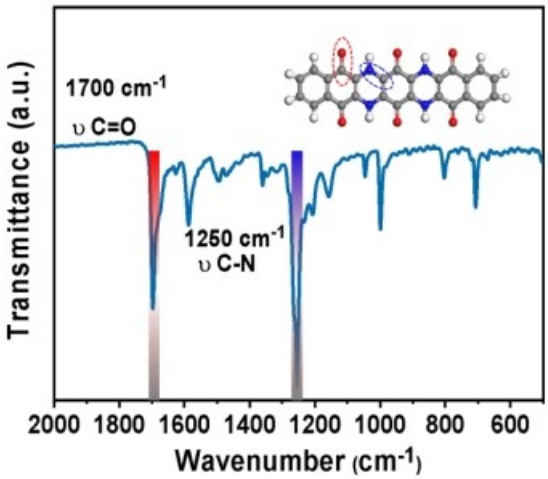

Figure S2 The FTIR of TBQPH material.

Figure S3.

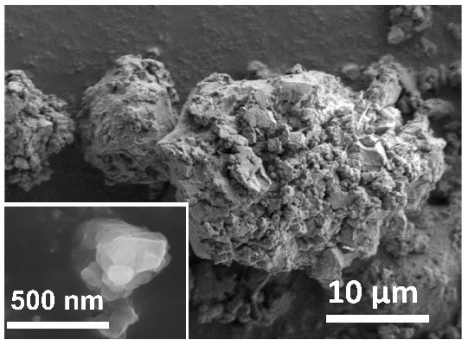

Figure S3 SEM image of TBQPH. Inset: zoom-in SEM image.

Figure S4.

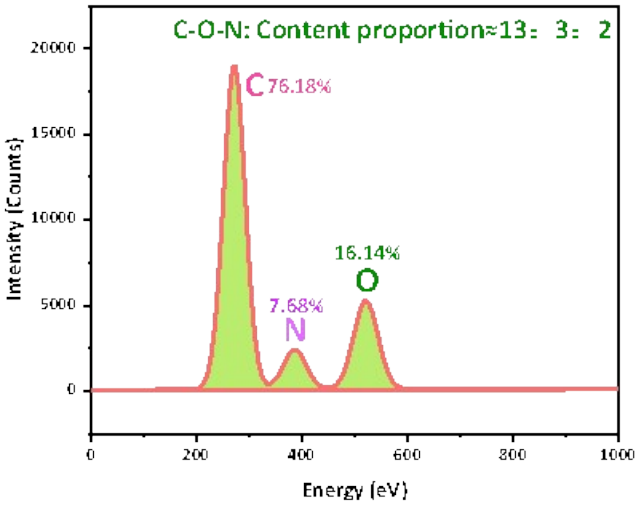

Figure S4 EDS plot of elemental distribution on the surface of TBQPH.

Figure S5.

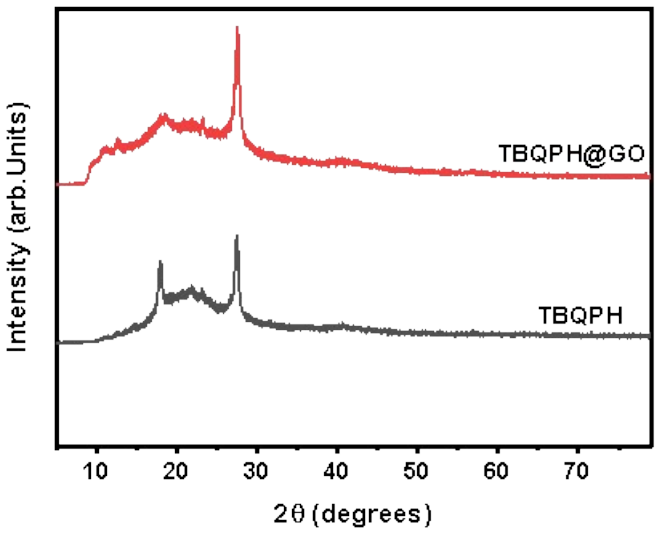

Figure S5 XRD images of TBQPH and TBQPH@GO

Figure S6.

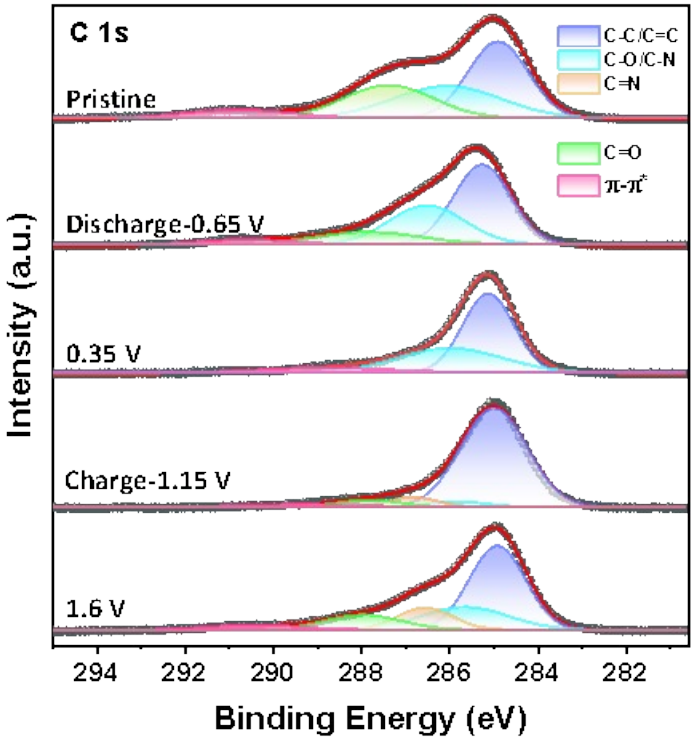

Figure S6 Fractionation of C 1s of TBQPH@GO//Zn cell on TBQPH@GO materials at different voltages.

Figure S7.

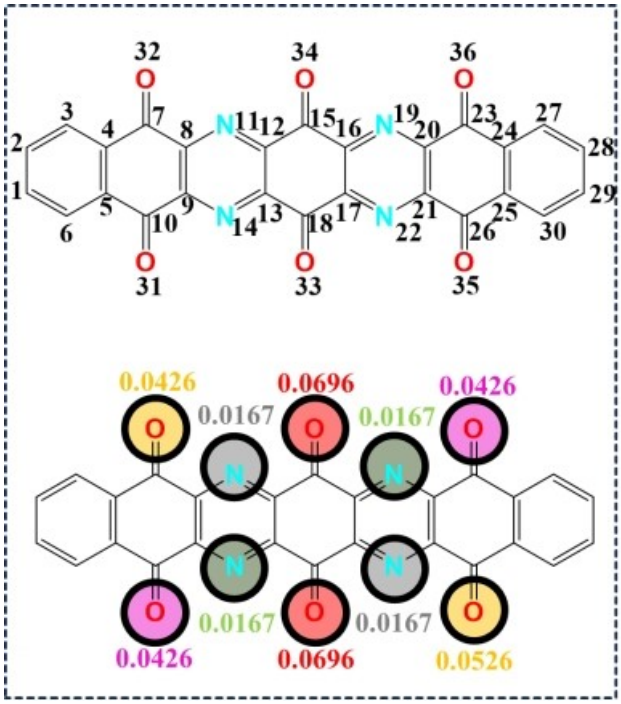

Figure S7 Fukui function (FUKUI) calculation of f^+ nucleophilic index on TBQPH surface.

Figure S8.

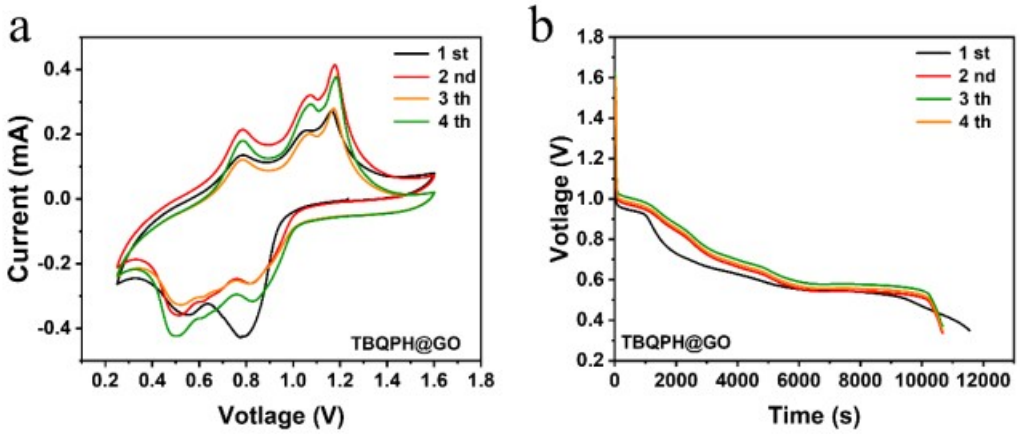

Figure S8 (a) CV and (b) GCD curves for the first four turns of the TBQPH//Zn cell.

Figure S9.

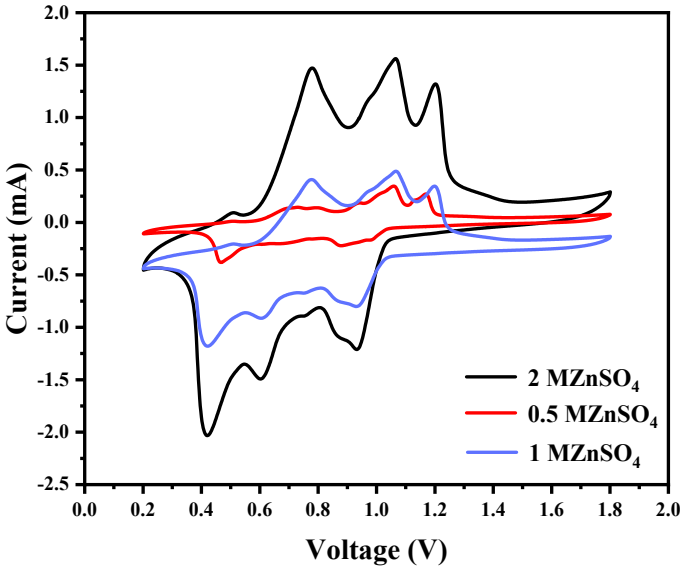

Figure S9 The CV curves of TBQPH@GO//Zn cells in electrolytes of varying concentrations.

Figure S10.

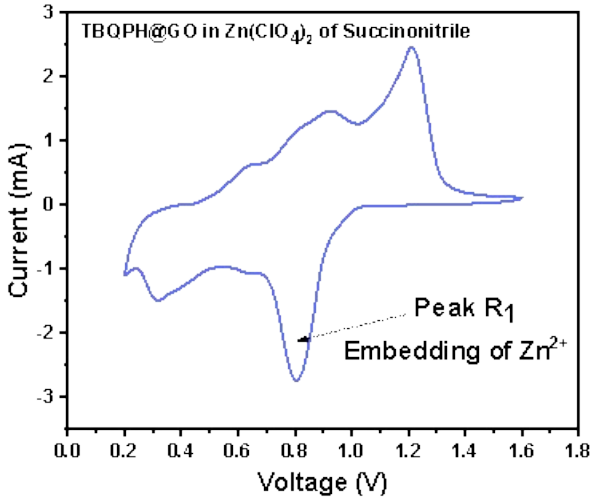

Figure S10 First lap CV curves of TBQPH@GO//Zn cells in Succinonitrile @ zinc perchlorate electrolyte.

Figure S11.

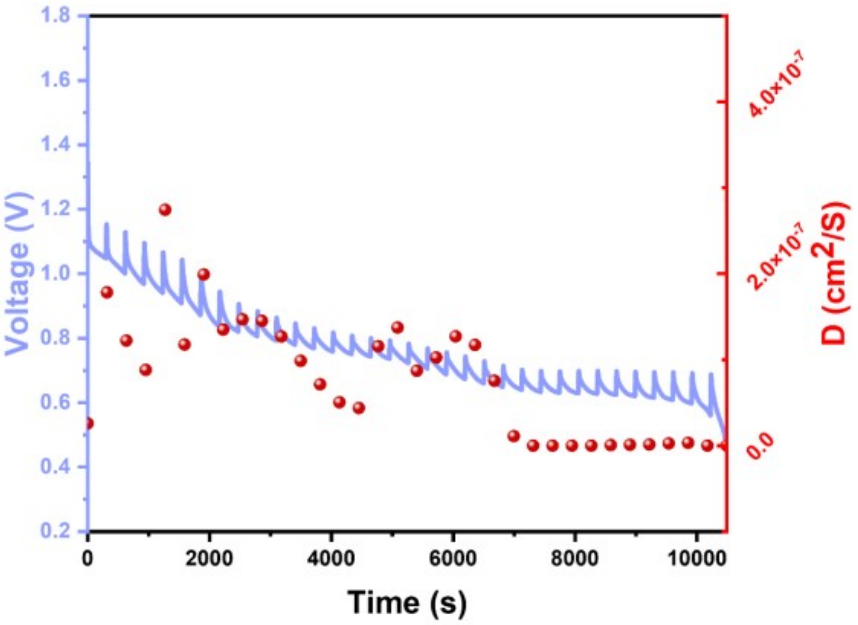

Figure S11 (a) GITT curve for TBQPH@GO//Zn cell discharge.

Figure S12.

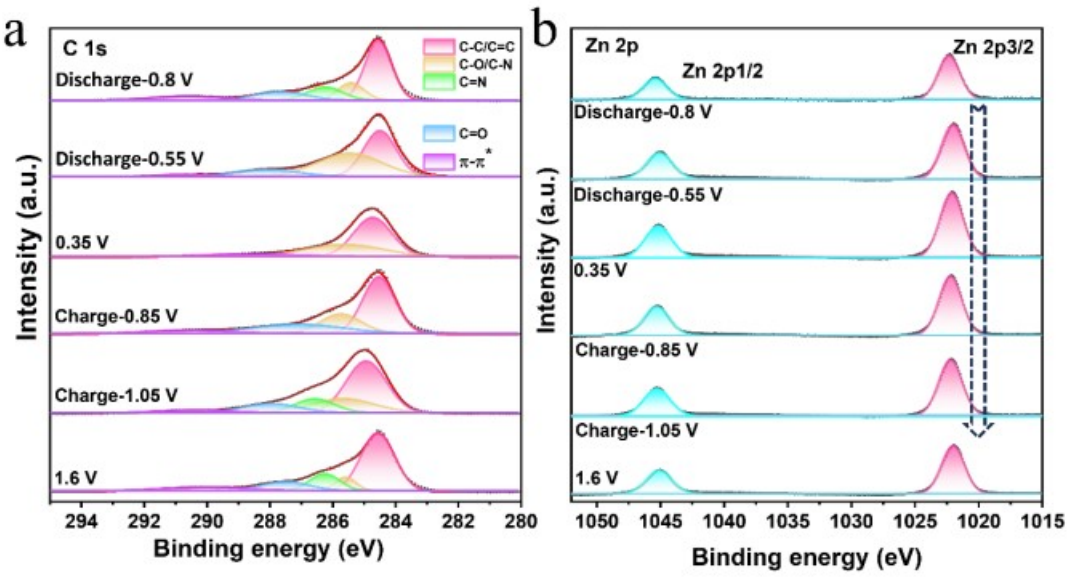

Figure S12 The effect of different voltages on the second cycle of Zn battery cycling TBQPH@GO Peaking of Material C 1s and Peaking of Zn 2p.

Figure S13.

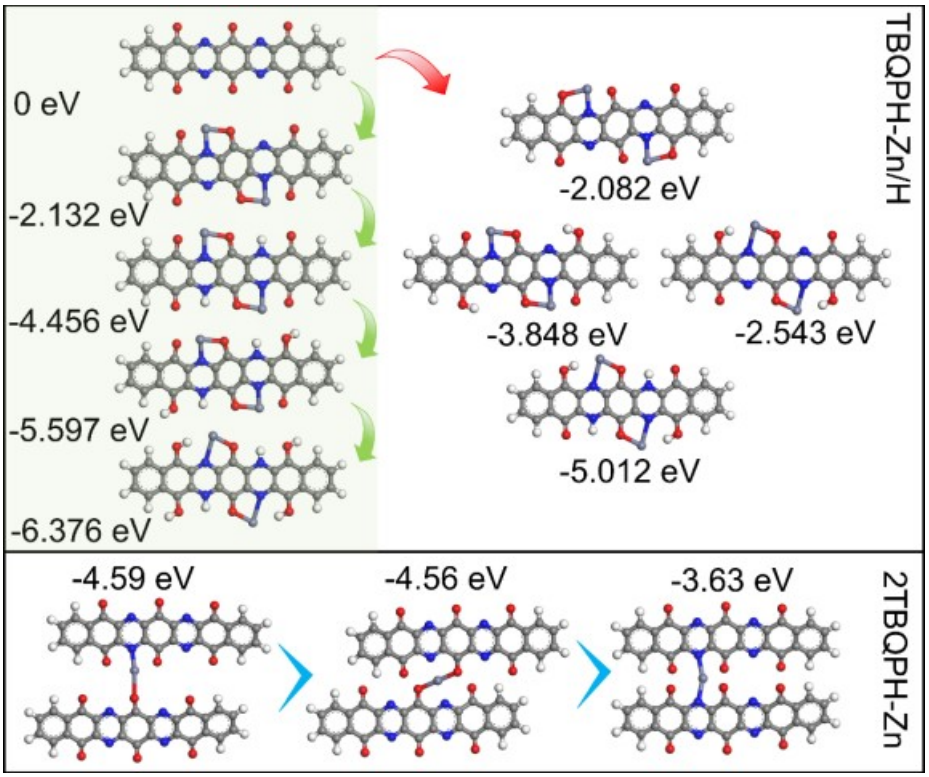

Figure S13 Comparison of Gibbs free energies of Zn^{2+}/H^{+} storage by TBQPH molecules and Zn^{2+} storage between TBQPH molecules.

Figure S14.

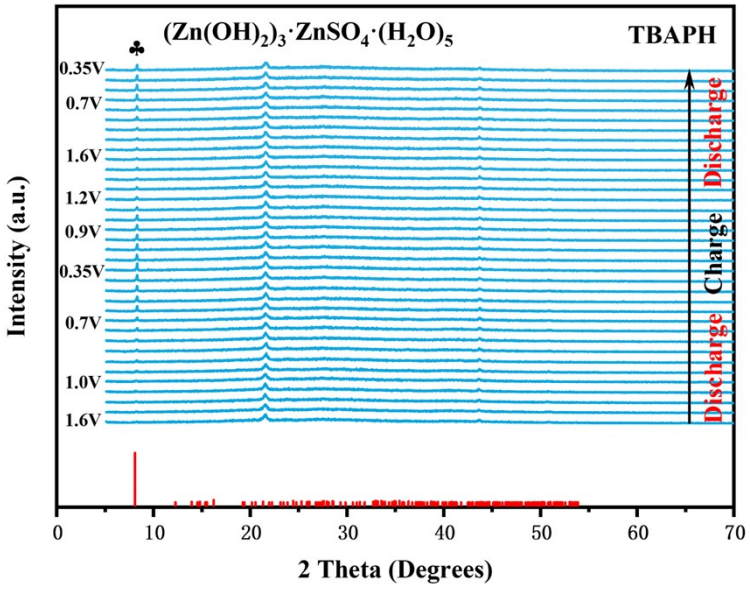

Figure S14 In-situ XRD of TBQPH during charge-diacharge.

Figure S15.

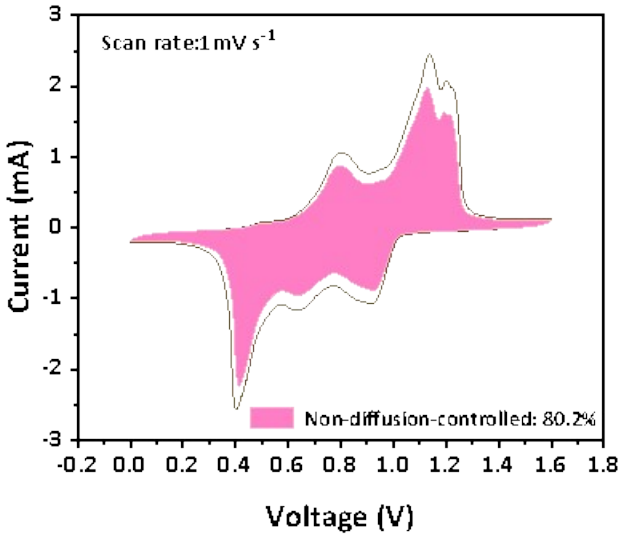

Figure S15 The non-diffusion-controlled region in the CV curve at 1 mV s^{-1}.

Figure S16.

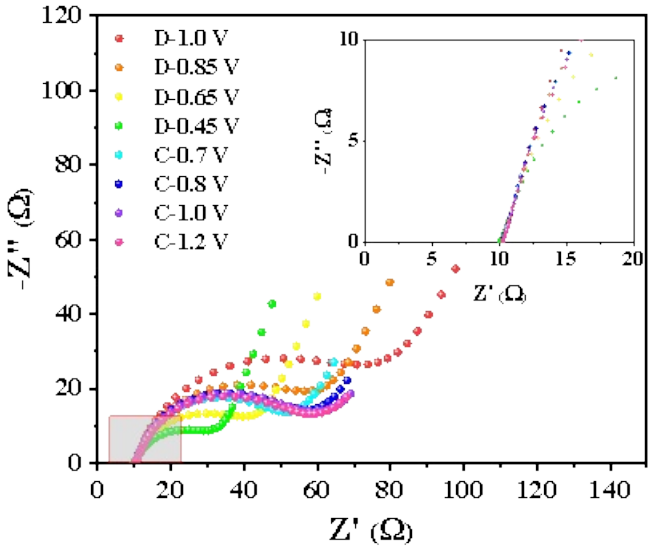

Figure S16 Nyquist plot obtained from battery impedance testing at different potentials during a single charge and discharge of TBQPH.

Figure S17.

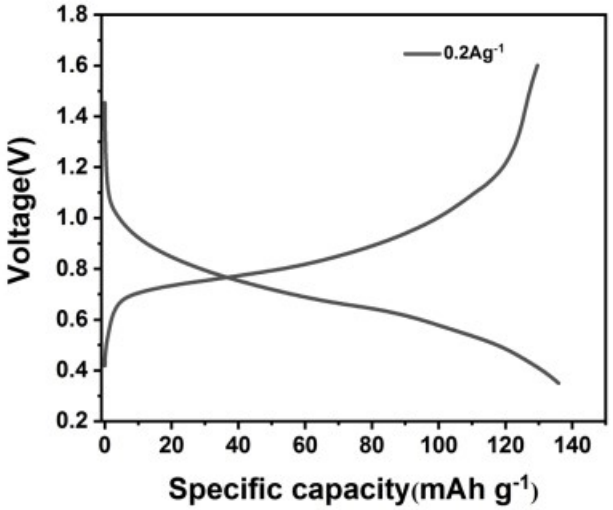

Figure S17 Capacity changes of TBQPH//Zn batteries at 0.2A g^{-1}.

Figure S18.

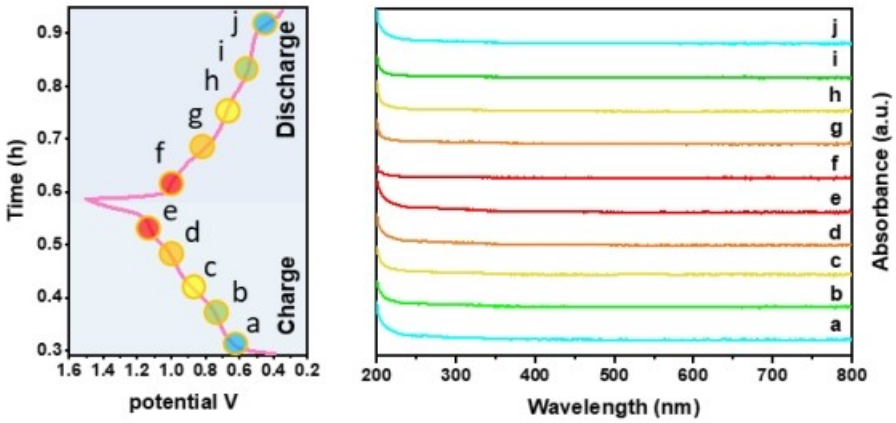

Figure S18 Ultraviolet analysis of electrolyte under different voltages during 1000 cycles of TBQPH@GO//Zn.

Figure S19.

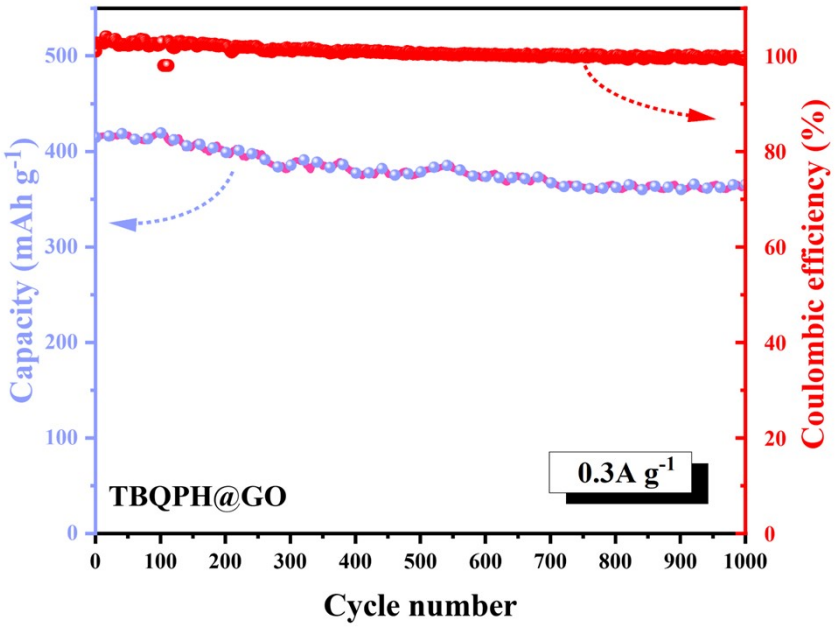

Figure S19 TBQPH@GO // Zn batteries at 0.3A g^{-1} current density.

Figure S20.

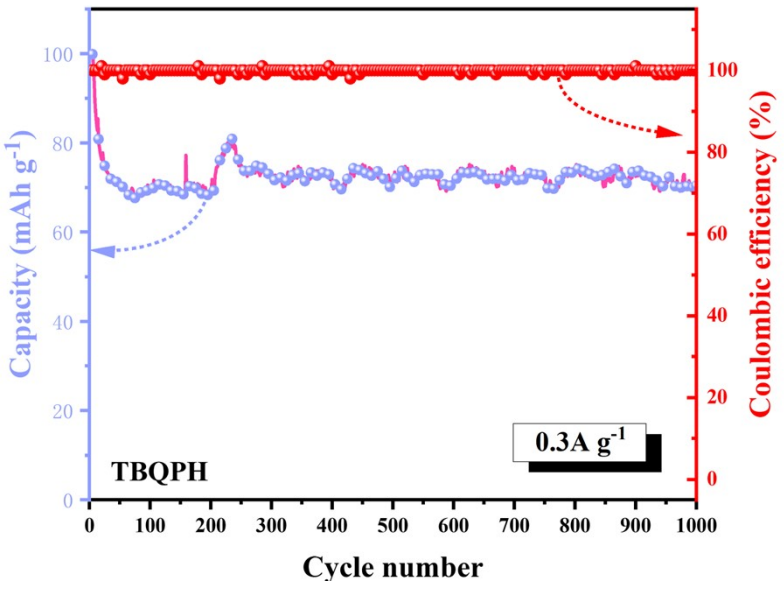

Figure S20 TBQPH //Zn batteries at 0.3A g^{-1} current density.

Figure S21.

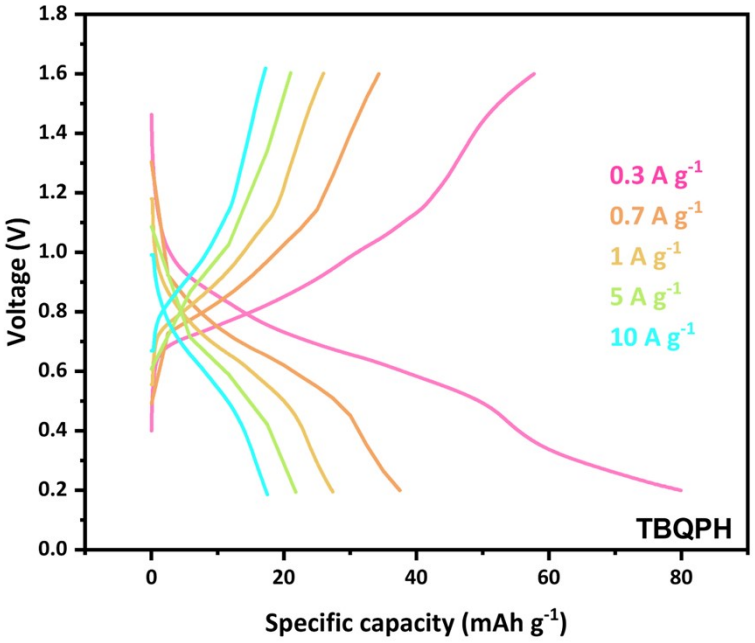

Figure S21 Rate performance of TBQPH //Zn batteries at various current densities.

Figure S22

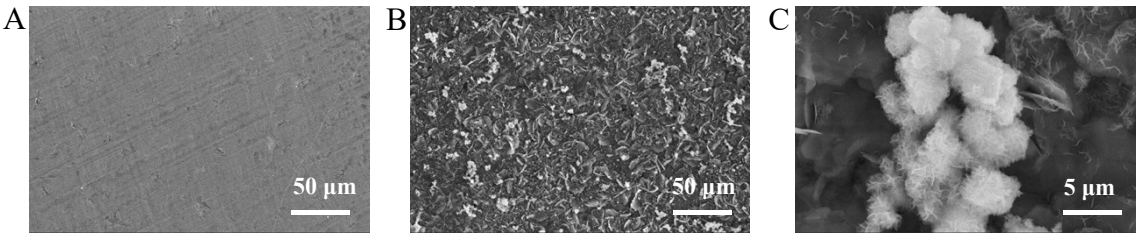

Figure S22. SEM images of the zinc anode surface in TBQPH @GO // Zn batteries before and after cycling: A) Before cycling, B) After cycling, C) Presence of basic zinc sulfate on the surface after cycling.

Figure S23

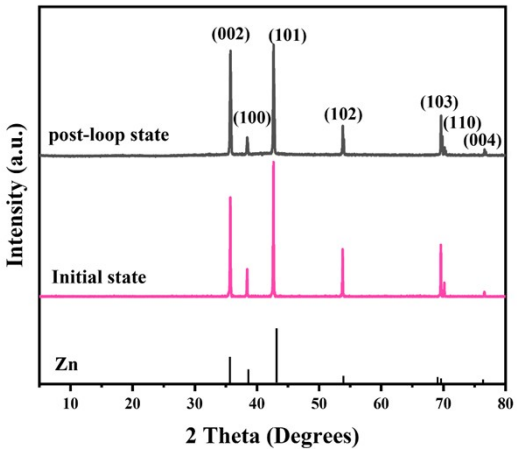

Figure S23. XRD patterns of the zinc anode surface in TBQPH @GO // Zn before and after cycling.

Figure S24

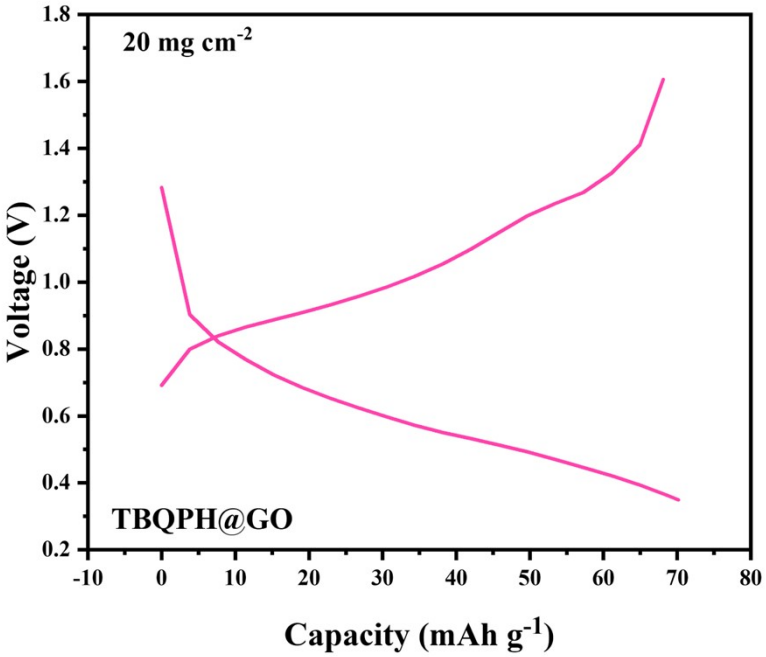

Figure S24. The charge-discharge curves of TBQPH@GO //Zn cell at a high loading of 20 mg cm^{-2} at 0.5 A g^{-1}.

Table S1.

T1 Fukui function (FUKUI) calculation of f^+ nucleophilic index on TBQPH surface

Atom	Change(0)(e/A^3)	Change(+1)(e/A^3)	Change(-1)(e/A^3)	f+
O-31	-0.2107	-0.2534	-0.152	0.0426
O-32	-0.2107	-0.2534	-0.1608	0.0426
O-33	-0.1845	-0.2541	-0.1406	0.0696
O-34	-0.1845	-0.2541	-0.1396	0.0696
O-35	-0.2107	-0.2534	-0.1577	0.0426
O-36	-0.2107	-0.2534	-0.1598	0.0426
N-11	-0.0929	-0.1096	-0.0503	0.0167
N-14	0.0929	-0.1096	-0.0525	0.0167
N-19	-0.0929	-0.1096	-0.0522	0.0167
N-22	-0.0929	-0.1096	-0.0528	0.0167

SI References

[1] Z. Ye, S. Xie, Z. Cao, L. Wang, D. Xu, H. Zhang, J. Matz, P. Dong, H. Fang, J. Shen, M. Ye, *Energy Storage Mater.* **2021**, 37, 378.

[2] Y. Gao, G. Li, F. Wang, J. Chu, P. Yu, B. Wang, H. Zhan, Z. Song, *Energy Storage Mater.* **2021**, 40, 31.

[3] C. Yin, C. Pan, Y. Pan, J. Hu, G. Fang, *Small Methods* **2023**, 7, 2300574.